Journal of Neuroscience Methods 211 (2012) 210–217

Contents lists available at SciVerse ScienceDirect

Journal of Neuroscience Methods

journal homepage: www.elsevier.com/locate/jneumeth

Computational Neuroscience

MRI-guided volume reconstruction of mouse brain from histological sections

Zhengyi Yang[a,b], Kay Richards[a,c], Nyoman D. Kurniawan[a,b], Steven Petrou[a,c,d], David C. Reutens[a,b,*]

[a] The Australian Mouse Brain Mapping Consortium, The University of Queensland, Brisbane, Australia
[b] Centre for Advanced Imaging, The University of Queensland, Queensland, Australia
[c] Florey Neuroscience Institutes, Parkville, Victoria, Australia
[d] Centre for Neuroscience, The University of Melbourne, Parkville, Victoria, Australia

HIGHLIGHTS

- A method of mouse brain histology reconstruction with the guidance of magnetic resonance images was presented.
- Magnetic resonance image was exploited to both constrain the overall shape of histology volume and correct intra-slice artifacts.
- Registration error was rigorously analysed by comparing corresponding anatomical landmarks on both magnetic resonance and histology volumes manually selected by experts.
- Four mouse brains were reconstructed using Nissl stained datasets and registration errors were found lower than those associated with potential error in defining the position of any point in a printed histological brain atlas.

ARTICLE INFO

Article history:
Received 30 March 2012
Received in revised form 22 August 2012
Accepted 23 August 2012

Keywords:
Histology reconstruction
Magnetic resonance image
Piecewise rigid registration

ABSTRACT

A method is presented for three-dimensional reconstruction of the mouse brain from histological sections with the guidance of magnetic resonance images (MRI). A major focus of the method is dealing with sections in which anatomical structures have been separated or distorted as a result of histological processing. Although histology has superb resolution with the ability to discriminate cell types and anatomical structures, misalignment between sections and distortion within sections renders 3D reconstruction of the histology volume simply by stacking 2D sections inadequate. In contrast, MRI preserves the spatial and geometric information about structures at a cost of cellular detail. To utilize the information from MRI in reconstructing volumetric histological data, we developed a procedure consisting of a series of segmentation and registration operations. The method is iterative and first identifies the corresponding MRI slices for each histological section. Piecewise rigid registration is then employed to deal with tissue distortion caused by histological processing. Quantitative validation of the method's accuracy was performed on four reconstructed mouse brains by comparing a set of manually selected anatomical landmarks on pairs of MRI and histological volumes. The procedure is highly automated and amenable to high throughput.

1. Introduction

Reconstruction of three-dimensional (3D) volumes from serial two-dimensional (2D) histological sections of the brain allows researchers to examine the microscopic counterparts of changes observed in 3D imaging methods such as MRI. Three-dimensional reconstruction also allows the spatial distribution of histological changes across the brain to be better appreciated (Bardinet et al., 2002; Malandain et al., 2004; Mansoori et al., 2007; Ourselin et al., 2001b; Yushkevich et al., 2006). Reconstruction by simply stacking registered histological sections does not yield results of adequate quality because of inter-section misalignment and intra-section imperfections caused by histological processing. The latter introduces nonlinear tissue distortions, such as separation, missing parts, squashing, stretching, folding and tearing, as well as artifacts including air bubbles and dust (Ju et al., 2006). Intensity inhomogeneity within and across sections caused by inconsistent staining and uneven illumination are other common issues. Examples of intra-section imperfections are shown in Fig. 1.

Methods of histological volume reconstruction reported in the literature can be broadly categorized into two groups according to whether a spatial reference containing inter-section geometric information was employed. In the early years of method development in this area, a spatial reference was not used and volume

* Corresponding author at: Centre for Advanced Imaging, The University of Queensland, Gehrmann Laboratory (Building 60), Research Road, St Lucia, QLD, 4072 Australia. Tel.: +61 7 3365 4237; fax: +61 7 3365 3833.
E-mail address: david.reutens@cai.uq.edu.au (D.C. Reutens).

0165-0270/$ – see front matter © 2012 Elsevier B.V. All rights reserved.
http://dx.doi.org/10.1016/j.jneumeth.2012.08.021

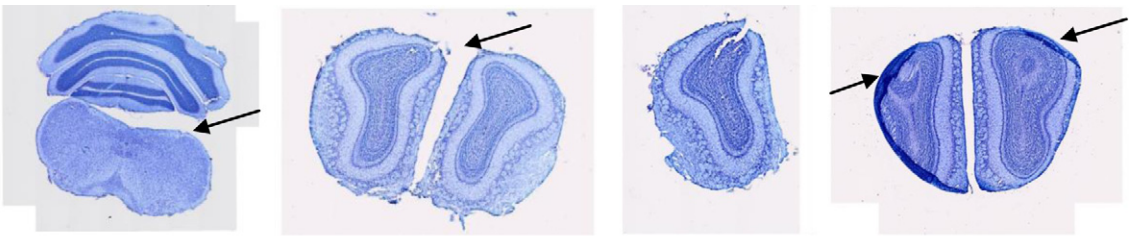

Fig. 1. Section imperfections: separated parts (a) and (b), half missing (c), and folding (d).

reconstruction from serial sections focused on finding the appropriate 2D registration algorithms for pairwise registration between consecutive sections. Registered sections were then stacked to form a 3D volume (Chakravarty et al., 2006; Ju et al., 2006; Kim et al., 1997; Ourselin et al., 2001a, 2001b). For example, the block matching algorithm was adapted to perform a local affine registration to account for non-rigid transformation across sections (Ourselin et al., 2001a, 2001b; Pitiot and Guimond, 2008). An inherent drawback of pairwise registration in the absence of an undistorted spatial reference is that good inter-section registration does not guarantee that overall brain shape will be accurately reconstructed because of error accumulation (Yushkevich et al., 2006). An accumulation of registration error can have the so-called 'banana' effect, which results in a linear structure being reconstructed as a spatial curve (Beare et al., 2008; Streicher et al., 1997). Smoothness-driven registration of histological sections achieves visually plausible volume reconstructions with continuous structures (Badea et al., 2007; Cifor et al., 2011, 2009; Wirtz et al., 2005), but because of the lack of an external reference the ability to overcome the 'banana' effect is unknown. In view of these limitations, recent studies utilize a spatial reference that maintains the spatial relationship between sections to guide the reconstruction process. Three classes of spatial reference that have been proposed are fiducial markers, block-face imaging and MRI images.

Fiducial markers have included holes drilled in the fixed tissue block before sectioning or external fiducials inserted into the block (Bardinet et al., 2002; Yelnik et al., 2007). Non-orthogonality of drilled holes can be problematic and holes drilled through tissue cause severe information loss (Beare et al., 2008). A volume formed from digitized images of the surface of the block during histological sectioning, 'block-face imaging', has been used as the 'ground truth' for creating the histology volume (Bürgel et al., 1999; Chakravarty et al., 2008a; Dauguet et al., 2007; Denk and Horstmann, 2004; Meyer et al., 2006; Schmitt et al., 2007; Schormann and Zilles, 1998; Uberti et al., 2009). Acquisition of block-face images complicates histological processing because of the extra equipment and handling required. As an alternative, high-resolution MR images have been proposed as a reference for histology reconstruction (Malandain et al., 2004; Yushkevich et al., 2006). Accurate registration of histology and MRI images also facilitates the analysis of complementary information from the two modalities. For example, histological volumes reconstructed utilizing the method described herein were used to evaluate track-density imaging (TDI), a novel super-resolution technique for diffusion MRI (Calamante et al., 2012).

The main challenge in using MR information to guide histology reconstruction is to find the slice from the MR volume corresponding to each histological section. The acquisition of the MR image in a different orientation to histology sections, a whole brain shrinkage or expansion during fixation and rehydration and deformation caused by sectioning make this a non-trivial task.

In this paper, we describe a method for high-resolution MRI-guided histological reconstruction and its rigorous quantitative validation in terms of the spatial localization error of anatomical landmarks in the two volumes. Our method employs an iterative strategy, motivated by previous work on histological reconstruction of the heart (Mansoori et al., 2007). Compared to work reported in literature (Malandain et al., 2004; Mansoori et al., 2007; Yushkevich et al., 2006), in which MRI was used to correct the overall shape only, our approach makes better use of MRI information to deal with both inter-section misalignment and major intra-section imperfections, such as separated parts. The global accuracy of registration between MRI and histology was directly measured by normalized mutual information and the local accuracy was validated by comparing corresponding anatomical landmarks on both MRI and histology volumes manually selected by experts.

2. Materials and method

In this study, histological sections of four C57BL/6J mice (12 week old males) brains were obtained as a subtask of building a mouse brain atlas. C57BL/6J is one of the most widely used strains of mice for scientific research and most mutant phenotypes are backcrossed onto this strain, making it a commonly used control/template strain (MacKenzie-Graham et al., 2003, 2004).

2.1. Image acquisition and preprocessing

The histology and MR images of four adult mouse brains (Brains 1–4) used in this study were acquired by the Australian Mouse Brain Mapping Consortium. Paraformaldehyde fixed samples were incubated with 0.1% Magnevist prior imaging inside the Fomblin medium (Solvey Solexis®). MR images were acquired using a 16.4T Bruker vertical NMR scanner (Bruker Biospin®, Germany) using the 3D gradient echo (FLASH) sequence with TR = 50 ms, TE = 12 ms, 30° flip angle, FOV = 22 mm × 11.5 mm × 8.5 mm. The voxel size of the acquired data and reconstructed images were identical at 30 μm in each dimension.

Subsequently, the brain samples were washed in phosphate buffer, cryoprotected using 20% sucrose and cut in a coronal plane using a microtome. For each brain, more than 350 Nissl-stained sections of 40 μm section thickness and in-plane resolution 0.65 μm × 0.65 μm were acquired. The images of the sections were taken using an Olympus® microscope and saved as JPEG colour images.

Both MR images and histological sections were converted to 8 bits gray-scale images for registration. The histological sections were down sampled to 1088 × 736 pixels with size 10.4 μm × 10.4 μm, to assure a computationally manageable image size. User intervention was required to construct a list of missing sections for each brain dataset and then the method proposed in literature (Qiu et al., 2009) was used to fill up the missing sections and missing parts and to correct folded sections. This method was unable to deal with separated parts. In our approach, the separated parts issue was solved by piecewise rigid registration (Section 2.4) within the iterative registration procedure described below.

Intensity inhomogeneity in histological sections was corrected using histogram equalization of each section to manually selected template sections.

2.2. Iterative registration method

To achieve a practical simplification of the problem, the histological sections were assumed to be of uniform thickness and to be parallel to each other. Shrinkage was assumed to occur mainly in the direction perpendicular to the sectioning planes. Based on these assumptions, a corresponding MR slice is found by re-orientating the MR volume into histological section space, followed by a search for the best matching MRI slice for any given histological section. Because the histological space is unavailable before reconstruction and the transformation of MR imaging space to histological space is unknown, we employ an iterative procedure to find the optimal transformation.

A flow chart for the method is shown in Fig. 2. The registration procedure is initiated by registering an MR volume to a subvolume of the histology image reconstructed using a set of consecutive sections containing no separated parts. This involves a series of 2D rigid registrations between adjacent histological sections indicated as Step A in Fig. 2. The identification of separated parts is described in Section 2.3. The entire MR volume is registered onto the subvolume using 6-parameter rigid registration (Step B) and the MR volume is resliced into histological space (Step C). Then, the MR slice that best matches each histological section is identified as that with the largest normalized mutual information (NMI) (Wells et al., 1996) when 2D rigid registration is performed between histology and each MR slice (Step D). To reduce computational time and to eliminate unlikely matches, the search for the best match is carried out in a neighbourhood only. The neighbourhood is defined by first identifying the corresponding MR slices for the first and last histological sections. This information is used to calculate a global linear shrinkage ratio in the rostral to caudal direction (which is perpendicular to the sectioning planes). Taking into account the global linear shrinkage ratio, linear interpolation is used to identify a candidate MR slice matching any given histological section. The search for the slice best matching each section is performed within a 30 slice neighbourhood (i.e. $30 \times 40 = 1200\,\mu m$ on each side) of this candidate MRI slice. The corresponding MRI and histological sections are then used to fix the problem of separated parts with a piecewise local rigid registration procedure (HtoM 2D LRR) described in Section 2.4.

Registered histological sections are then stacked to form an estimate of the histology volume (Step E), onto which MR volume again is registered (Step B). The procedure is repeated until the MRI-histology transformation matrix stabilizes, defined operationally as changes in translation and rotation falling below 200 μm in each dimension and 1 degree along each axis, respectively. The initial registrations of MRI to histology are rigid and when the stability criteria are reached (generally within three iterations), in Step F, non-rigid registration is employed to warp the histology volume to the MR volume using MIPAV (2012).

2.3. Automatic segmentation of histological sections

Segmentation is necessary because of the noisy background in histological sections caused by staining artifact, such as debris, bubbles, and the edges of the coverslip (Yushkevich et al., 2006). We remove background noise by adaptive thresholding (Otsu, 1979). In our approach, segmentation is also used to automatically identify separated parts. Morphological operations consisting of dilation and erosion followed by connectivity analysis are used to create masks for each separated part. Thresholding is required to remove any negligible debris. Hence, for any section the largest four connected regions with an area larger than a threshold value are regarded as objects. The threshold value we use for minimum area is 1% of the largest region on the same section. An example of separated parts identification is given in Fig. 3. Missing sections are identified based on experimental record of histology procedure and automatically appended by interpolation between adjacent sections.

2.4. Piecewise local rigid registration

Although strict quality control may reduce the occurrence of separated parts during tissue sectioning and staining, the problem is unlikely to be entirely eliminated. Previously, separated parts have been dealt with by averaging several histological volumes (Li et al., 2009) or by discarding poor quality sections to prevent them from hindering reconstruction. However, these approaches may lead to important information being lost. Nonlinear warping of the histological section as a whole to the MR slice or to adjacent sections has also been proposed but introduces errors. We propose a piecewise local rigid registration (LRR) method to solve this problem so as to minimise loss of information contained in histological sections (Yang et al., 2010).

When performing 2D registrations of histological sections to MR slices, as in Step D in Fig. 2, each separated part is treated as a rigid body with independent degrees of freedom to move. The registration seeks a set of transformation matrices for the separated parts to maximize the similarity between the combined histological section and the corresponding MR image. Normalized mutual information is used as the similarity metric. In conventional 2D rigid-body registration, 3 parameters (2 translational and 1 rotational) are optimized. Thus, the number of parameters in this multi-part approach is equal to 3 times the number of separated parts. We use Stochastic Differential Evolution Optimization, a global optimization method, to identify the optimal parameters (Vegh et al., 2010). In Fig. 4, an example of piecewise rigid registration is illustrated. Two separated parts were identified on the histological section and an independent rigid transformation was found for each to be co-registered to the same MR slice. On the checker board view, it can be observed that the internal structures were aligned well. It would be difficult to recover the dislocation of the separated part if an affine followed by a non-linear registration is applied to the whole histological section.

All the segmentation and registration processes (Steps A to E) are performed using dedicated software written in Matlab®, except for the 3D non-linear registration of the volumes (Step F), which is conducted in MIPAV (2012). In the 3D warping, cubic B-splines are employed to model the deformation field and the normalized correlation coefficient is the similarity metric used.

2.5. Validation

To estimate the registration error of the proposed method, 30 landmarks were randomly placed in the MR images. Three experts (KR, NK, and DR) then identified the corresponding locations on the reconstructed histological volumes on two occasions (Trial 1 and Trial 2) separated by at least a month using the software Display (MINC suite). This resulted in 720 pairs of locations, with 360 pairs in each trial. The Euclidean distance between the corresponding locations was calculated as the registration error. Analysis of variance (ANOVA) was used to partition the total variance into components caused by inter- and intra- observer variability and by differences between individual brains.

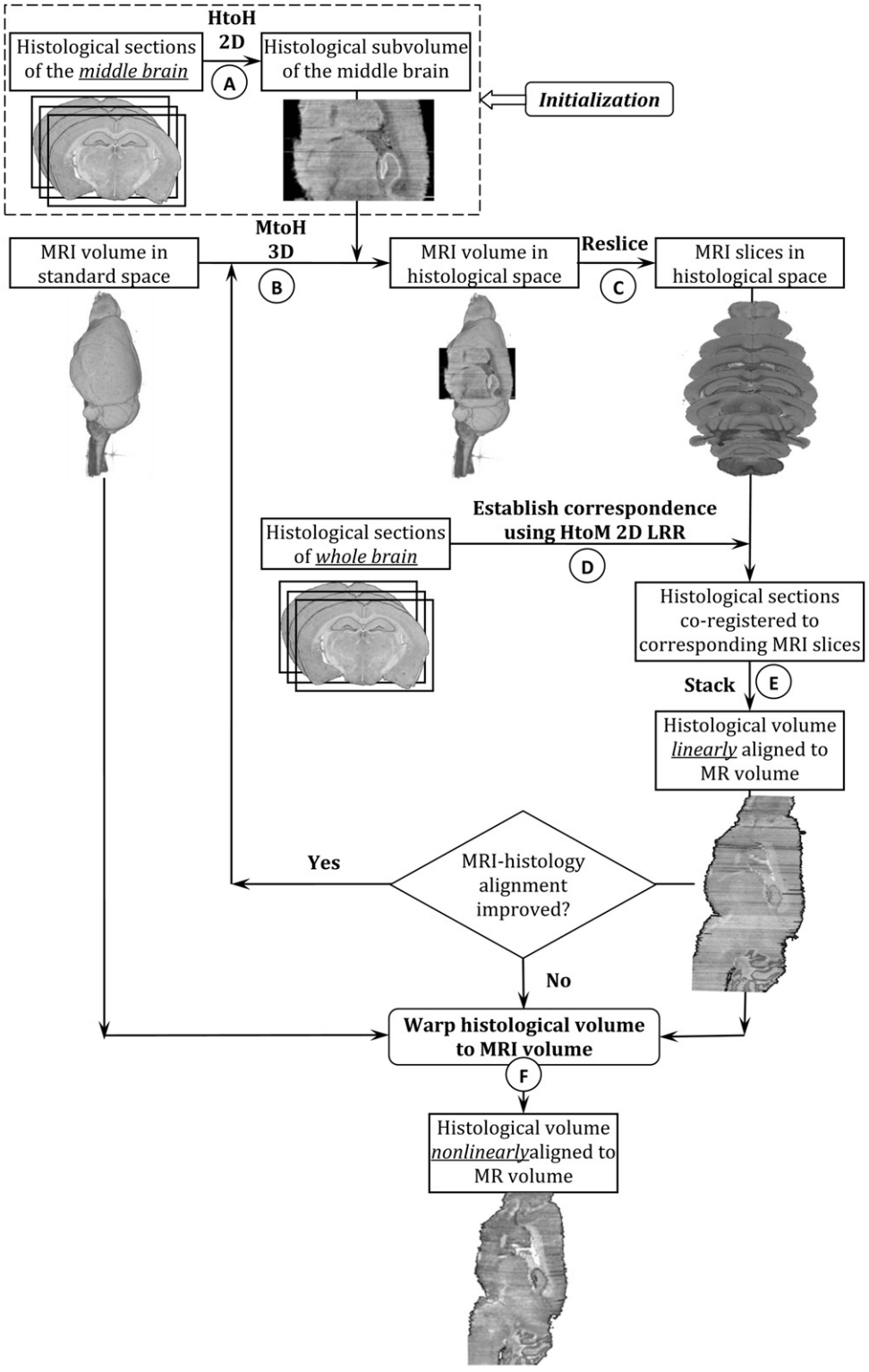

Fig. 2. Iterative method used to establish the correspondence between MR slices and histological sections. HtoH: histology to histology; HtoM: histology to MRI; MtoH: MRI to histology.

3. Results and discussion

Table 1 illustrates the magnitude of problem imposed by histological artifacts. Our method of piecewise local rigid registration handled the sections with and without separated parts automatically. By visual inspection, all the pairs appeared to be satisfactorily registered and no sections were discarded because of inability to correct the separated parts artifact. As an indicator of the quality of registration, the mean and standard deviation values of NMI between each pair for each brain at the end of each iteration is shown in the second column in Table 2. Registration time for individual 2D pairs varied from 1 to 5 min. Sections from a histology volume and the corresponding MRI image used to reconstruct it are available at http://www.imaging.org.au/AMBMC/histrecon.

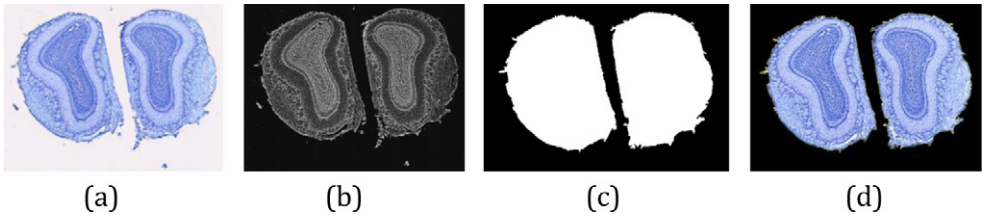

Fig. 3. An example of identifying separated parts by segmentation. (a) original histological section; (b) background removed and turned into gray-scale image; (c) masks created by morphological operations and connectivity analysis; (d) separated parts identified and debris removed. (For interpretation of the references to colour in Figure legend, the reader is referred to the web version of the article.)

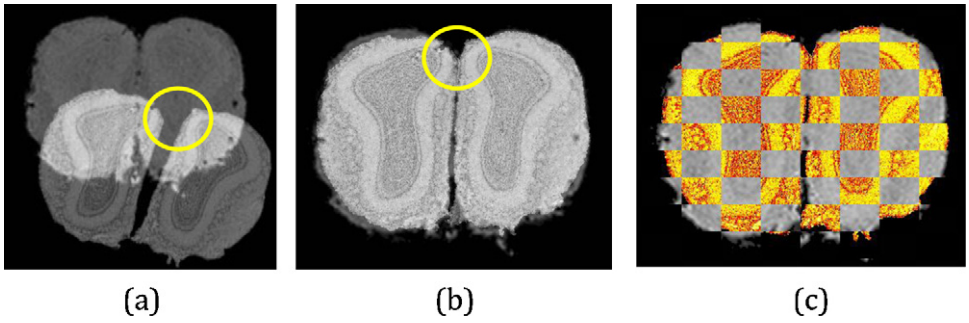

Fig. 4. An example of piecewise rigid registration of histological sections to MR slices. (a) before registration; (b) after registration; (c) checker-board view of the co-registered images (histology in colour and MR in gray-scale).

Table 1
Histological artifacts in brains used in this study. The total number of sections after inserting missing sections is shown in the second column. The difference between the numbers of total and missing sections is the number of sections available in the raw dataset. A section is considered to have separated parts when there is more than one connected piece in that section.

Brain ID	Total	Missing	Separated parts	Folding
1	426	9	267	11
2	381	41	69	3
3	416	40	36	1
4	401	42	130	3

The result of iterative piecewise rigid registration for Brain 1 is illustrated in Fig. 5 and demonstrates obvious shrinkage of the histology volume. In Fig. 5(c), the serial numbers of histological sections are plotted against that of the corresponding MRI slices and the data was fitted with a straight line. The linear relationship between the spacing of corresponding histology and MR slices in the rostral to caudal direction supports our method of using linear interpolation between MR slices corresponding to the first and the last histological sections to initialize the search for the MR slice which best matches each histological section. The inter-slice intensity inhomogeneity corrected and nonlinearly aligned histology volume resulting from the final reconstruction is shown in Fig. 6.

Table 2
Quantitative measures of registration quality in brains studied (denoted by ID). The means and standard deviations of NMI values between the corresponding histological sections and MR slices over iterations are listed in column 3. NMI values between the reconstructed histological volume and MR volume and the change in transformation parameters over iterations are listed in columns 4–6. Iteration 0 represents the initialization step: registration of MR to histology subvolume reconstruction. 'Warping' is the final 3D non-linear registration. The shrinkage ratio is the ratio between the rostro-caudal length of the histological image and that of the MR image.

ID	Iteration	NMI (2D)	NMI (3D)	3D Translation (mm)	3D Rotation (degree)	Shrinkage
1	0	–	0.9028	−0.021, 0.822, −2.505	12.984, 1.120, −0.247	–
	1	0.832 ± 0.013	0.9148	0.333, 2.729, −1.932	15.007, −1.769, −2.776	0.8893
	2	0.877 ± 0.019	0.9192	0.046, 3.745, −1.780	14.700, 2.125, −1.805	0.8875
	3	0.901 ± 0.018	0.9201	0.031, 3.702, −1.648	14.385, 1.947, −1.881	0.8854
	Warping	–	0.8644	–	–	–
2	0	–	0.9154	0.593, −2.860, 3.443	13.084, 3.937, 1.048	–
	1	0.783 ± 0.014	0.9160	−0.483, 1.590, 1.329	11.383, 1.826, 2.412	0.9182
	2	0.880 ± 0.014	0.9230	0.119, −0.050, −0.096	11.949, −0.003, 3.921	0.8978
	3	0.896 ± 0.009	0.9267	0.104, −0.035, −0.111	12.390, 0.308, 3.007	0.9168
	Warping	–	0.8799	–	–	–
3	0	–	0.8910	−1.740, 1.038, −0.394	−7.008, 1.204, 1.555	–
	1	0.794 ± 0.015	0.9156	1.578, −1.994, −1.243	−9.979, 1.033, 1.839	0.7393
	2	0.821 ± 0.013	0.9243	−0.159, 0.379, −2.900	−8.202, 1.693, 1.005	0.7924
	3	0.879 ± 0.013	0.9270	−0.143, −0.380, −2.886	−8.911, 2.097, 1.226	0.8102
	Warping	–	0.9023	–	–	–
4	0	–	0.9035	2.197, −1.303, 3.886	6.586, 2.477, −1.398	–
	1	0.895 ± 0.011	0.9200	1.109, 1.333, 4.100	10.562, 1.223, 0.865	0.9643
	2	0.900 ± 0.009	0.9114	−0.030, 0.569, 4.091	11.225, 1.236, 1.473	0.9526
	3	0.903 ± 0.008	0.9268	−0.014, 0.586, 4.084	12.219, 1.243, 0.971	0.9291
	Warping	–	0.9115	–	–	–

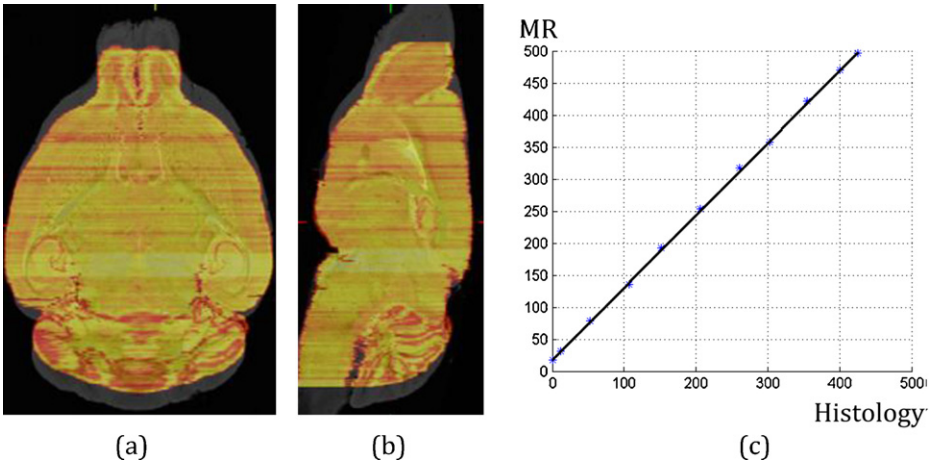

Fig. 5. Result of iterative rigid registration (Step E in the last iteration). MR image (in gray-scale) and histology image (in hot-metal colour) are superimposed. (a) axial view; (b) sagittal view; (c) the corresponding MR slices found for histological section demonstrated a linear shrinkage in the rostral to caudal direction.

Because the 'ground truth' from un-sectioned tissue is often unknown, accuracy of reconstruction has often been assessed qualitatively, for example by assessing the smoothness of the contours of reconstructed anatomical structures. The projections of the surface reconstruction in three orthogonal directions (Schormann et al., 1993) and a comparison of MR atlas-based and manual segmentation of structures of interest in reconstructed histology volumes (Chakravarty et al., 2008b; Lebenberg et al., 2010) have been used

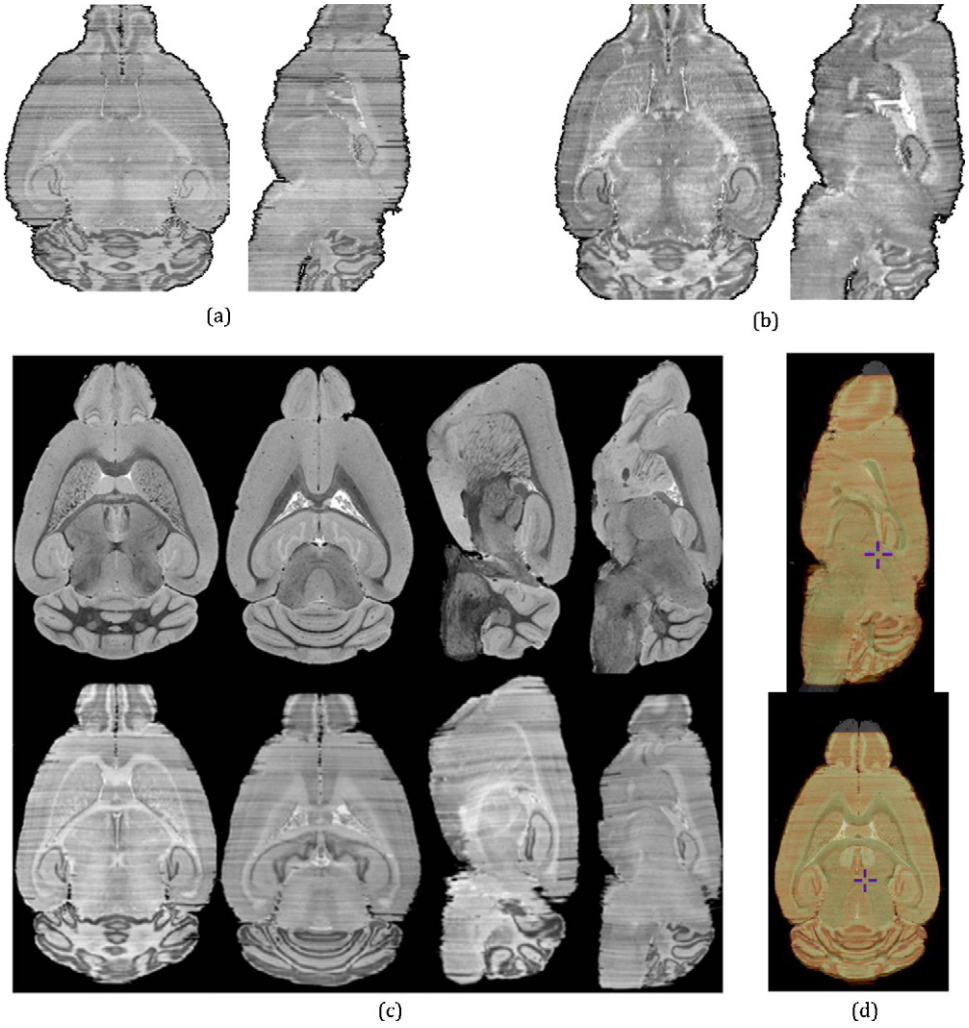

Fig. 6. The axial and sagittal views of reconstructed histological volume, before (a) and after (b) intensity inhomogeneity correction and warping to MR volume. Axial and sagittal views of reconstructed histology volume (bottom row) and corresponding MR slices (top row) are shown in (c). The superimposed histological volume (in colour) and the MRI volume (in grayscale) are shown in (d). The images are of Brain 1.

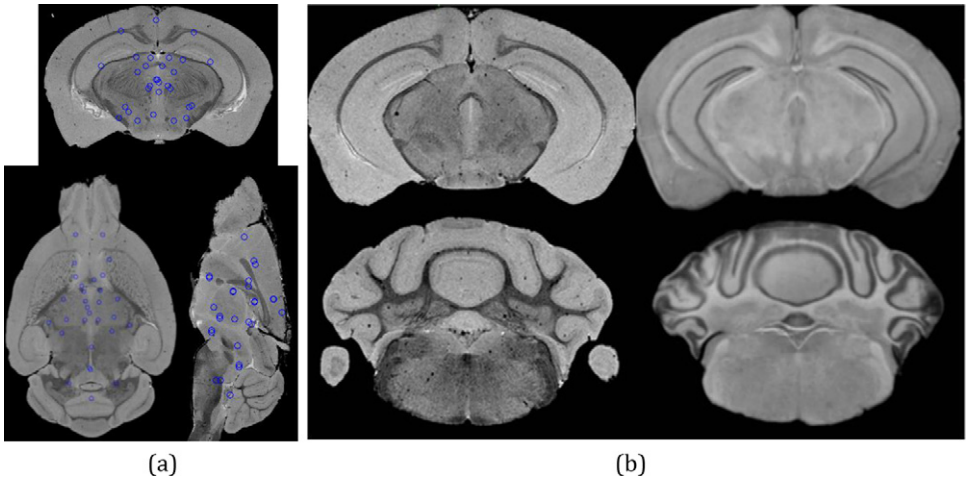

Fig. 7. (a) 3D landmarks used for validation projected on 2D MRI slices. (b) coronal view of example corresponding slices.

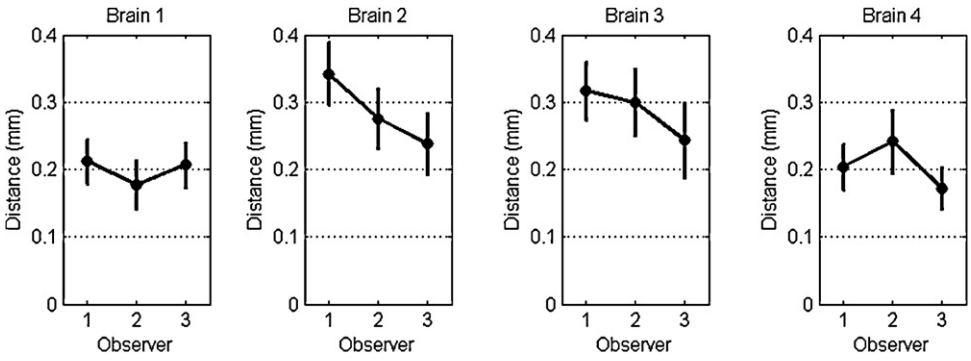

Fig. 8. The mean and 95% confidence interval of the measurements of the three experts on each brain.

to evaluate registration errors quantitatively. Instead of using segmentation accuracy to infer registration error, we estimated the registration error directly from repeated measurements of the discrepancy between landmark locations on the histology-MR volume pairs in the same reference space. One sample set of landmarks used for validation has been projected on the tri-planar view of the corresponding MRI volume (Brain 1) in Fig. 7(a).

The mean Euclidean distance for all pairs is 0.27 ± 0.14 mm, equivalent to 9.0 ± 4.5 voxels. This value contains registration error caused by the method itself as well as errors made by the raters. The mean Euclidean distance for all raters was 0.29 ± 0.15 in Trial 1 and 0.24 ± 0.12 in Trial 2 and was statistically significant ($p < 0.001$) implying a learning effect for the manual raters.

For each trial, a two-way ANOVA with main effects of observer and brain and their interactions was carried out. Significant interactions were found in both trials (Trial 1: $p = 0.0002$ and Trial 2: $p = 0.0309$). Therefore, one-way ANOVA was performed on the dataset for each mouse brain in each trial. This demonstrated a significant effect of rater ($p < 0.05$). The mean Euclidean distance for each rater in individual brains for Trial 2 is illustrated in Fig. 8.

Given the significant learning effect, the best estimate of registration error is provided by data from Trial 2 and is given by the mean Euclidean distance as shown in Table 3. Means for each observer ranged from 0.20 mm to 0.29 mm, the maximum upper bound of the 95% confidence interval was 0.31 mm and the minimum lower bound of the 95% confidence interval was 0.18 mm. The bounds of registration error are lower than the potential error in defining the position of any point on a widely used histological atlas which is 0.5 mm (Paxinos and Watson, 2007).

Table 3
The mean and 95% confidence intervals (CI) of measurements of the three experts on each brain in the second trial.

Brain ID	Mean (mm)	CI of mean (mm)
1	0.1985	[0.1797, 0.2173]
2	0.2849	[0.2585, 0.3113]
3	0.2865	[0.2585, 0.3144]
4	0.2057	[0.1844, 0.2270]

Options for future work to improve the method include incorporating the block-matching algorithm (Zhu and Ma, 2000) for non-rigid affine registration after piece-wise registration. Isotropic shrinkage within sections is assumed in our method, however, different tissue type could have different shrinkage ratios and how this information could be exploited to improve the reconstruction requires investigation. The application of the proposed method to other histological stains and to the brains of other species also requires validation. We also note that differences in staining intensity between sections could be removed by more sophisticated intensity normalization methods, such as those reported in literature (Chakravarty et al., 2006; Malandain and Bardinet, 2003; Malandain et al., 2004). Given the intensity inhomogeneity between slices in MR is generally less pronounced that with histology, one option is an MR-guided intensity normalization step in the iterative reconstruction algorithm.

4. Conclusion

Three-dimensional reconstruction of serial histological sections and registration with high resolution MRI allows the shapes,

cellular and histochemical characteristics of structures to be analysed to an extent not possible with individual sections (Bjaalie and Leergaard, 2006). Our MRI-guided histology volumetric reconstruction method has been tested on real MRI and Nissl stained datasets and registration errors are lower than those associated with potential error in defining the position of any point in a histological brain atlas. The novel use of piecewise rigid registration integrated into an iterative procedure, allows high-resolution MRI to be employed to correct both global shape distortion and major intra-slice artifacts.

Acknowledgment

This work was supported by the National Health and Medical Research Council of Australia.

References

MIPAV, 2012. http://mipav.cit.nih.gov/

Badea A, Ali-Sharief AA, Johnson GA. Morphometric analysis of the C57BL/6J mouse brain. NeuroImage 2007;37:683–93.

Bardinet É, Ourselin S, Dormont D, Malandain G, Tandé D, Parain K, Ayache N, Yelnik J. Co-registration of histological, optical and MR data of the human brain. In: International conference on medical image computing and computer-assisted intervention; 2002. p. 548–55.

Beare R, Richards K, Murphy S, Petrou S, Reutens DC. An assessment of methods for aligning two-dimensional microscope sections to create image volumes. J Neurosci Methods 2008;170:332–44.

Bjaalie JG, Leergaard TB. Three-dimensional computerized reconstruction from serial sections: cell populations, regions, and whole brain. In: Neuroanatomical Tract-Tracing; 2006. p. 530–65.

Bürgel U, Schormann T, Schleicher A, Zilles K. Mapping of histologically identified long fiber tracts in human cerebral hemispheres to the MRI volume of a reference brain: position and spatial variability of the optic radiation. NeuroImage 1999;10:489–99.

Calamante F, Tournier J-D, Kurniawan ND, Yang Z, Gyengesi E, Galloway GJ, Reutens DC, Connelly A. Super-resolution track-density imaging studies of mouse brain: comparison to histology. NeuroImage 2012;59:286–96.

Chakravarty MM, Bedell BJ, Zehntner SP, Evans AC, Collins DL. Three-dimensional reconstruction of serial histological mouse brain sections. In: The 5th IEEE international symposium on biomedical imaging: from nano to macro; 2008a. p. 987–90.

Chakravarty MM, Bertrand G, Hodge CP, Sadikot AF, Collins DL. The creation of a brain atlas for image guided neurosurgery using serial histological data. NeuroImage 2006;30:359–76.

Chakravarty MM, Sadikot AF, Germann J, Bertrand G, Collins DL. Towards a validation of atlas warping techniques. Med Image Anal 2008b;12:713–26.

Cifor A, Bai L, Pitiot A. Smoothness-guided 3-D reconstruction of 2-D histological images. Neuroimage 2011;56:197–211.

Cifor A, Pridmore T, Pitiot A. Smooth 3-D reconstruction for 2-D histological images. In: The 21st international conference on information processing in medical imaging; 2009. p. 350–61.

Dauguet J, Delzescaux T, Conde F, Mangin JF, Ayache N, Hantraye P, Frouin V. Three-dimensional reconstruction of stained histological slices and 3D non-linear registration with in vivo MRI for whole baboon brain. J Neurosci Methods 2007;164:191–204.

Denk W, Horstmann H. Serial block-face scanning electron microscopy to reconstruct three-dimensional tissue nanostructure. PLoS Biol 2004;2:1900–9.

Ju T, Warren J, Carson J, Bello M, Kakadiaris I, Chiu W, Thaller C, Eichele G. 3D volume reconstruction of a mouse brain from histological sections using warp filtering. J Neurosci Methods 2006;156:84–100.

Kim B, Boes JL, Frey KA, Meyer CR. Mutual information for automated unwarping of rat brain autoradiographs. NeuroImage 1997;5:31–40.

Lebenberg J, Hérard AS, Dubois A, Dauguet J, Frouin V, Dhenain M, Hantraye P, Delzescaux T. Validation of MRI-based 3D digital atlas registration with histological and autoradiographic volumes: an anatomofunctional transgenic mouse brain imaging study. NeuroImage 2010;51:1037–46.

Li X, Yankeelov TE, Rosen GD, Gore JC, Dawant BM. Enhancement of histological volumes through averaging and their use for the analysis of magnetic resonance images. Magn Reson Imaging 2009;27:401–16.

MacKenzie-Graham A, Jones E, Shattuck D, Dinov I, Bota M, Toga A. The informatics of a C57BL/6J mouse brain atlas. Neuroinformatics 2003;1:397–410.

MacKenzie-Graham A, Lee EF, Dinov ID, Bota M, Shattuck DW, Ruffins S, Yuan H, Konstantinidis F, Pitiot A, Ding Y. A multimodal, multidimensional atlas of the C57BL/6J mouse brain. J Anat 2004;204:93.

Malandain G, Bardinet E. Intensity compensation within series of images. In: The international conference on medical image computing and computer-assisted intervention; 2003. p. 41–9.

Malandain G, Bardinet E, Nelissen K, Vanduffel W. Fusion of autoradiographs with an MR volume using 2-D and 3-D linear transformations. NeuroImage 2004;23:111–27.

Mansoori T, Plank G, Burton R, Schneider J, Kohl P, Gavaghan D, Grau V. An iterative method for registration of high-resolution cardiac histoanatomical and MRI images. The 4th IEEE international symposium on biomedical imaging: from nano to macro 2007:572–5.

Meyer CR, Moffat BA, Kuszpit KK, Bland PL, McKeever PE, Johnson TD, Chenevert TL, Rehemtulla A, Ross BD. A methodology for registration of a histological slide and in vivo MRI volume based on optimizing mutual information. Mol Imaging 2006;5:16–23.

Otsu N. A threshold selection method from gray-level histograms. IEEE Trans Syst Man Cybern B Cybern 1979;9:62–6.

Ourselin S, Bardinet E, Dormont D, Malandain G, Roche A, Ayache N, Tandé D, Parain K, Yelnik J. Fusion of histological sections and MR images: towards the construction of an atlas of the human basal ganglia. In: The international conference on medical image computing and computer-assisted intervention; 2001a. p. 743–51.

Ourselin S, Roche A, Subsol G, Pennec X, Ayache N. Reconstructing a 3D structure from serial histological sections. Image Vis Comput 2001b;19:25–31.

Paxinos G, Watson C. The rat brain in stereotaxic coordinates. Boston: Academic Press; 2007.

Pitiot A, Guimond A. Geometrical regularization of displacement fields for histological image registration. Med Image Anal 2008;12:16–25.

Qiu X, Pridmorea T, Pitiotb A. Correcting distorted histology slices for 3D reconstruction. In: The 13th international conference on medical image understanding and analysis; 2009. p. 224–8.

Schmitt O, Modersitzki J, Heldmann S, Wirtz S, Fischer B. Image registration of sectioned brains. Int J Comput Vis 2007;73:5–39.

Schormann T, von Matthey M, Dabringhaus A, Zilles K. Alignment of 3-D brain data sets originating from MR and histology. Bioimaging 1993;1:119–28.

Schormann T, Zilles K. Three-dimensional linear and nonlinear transformations: an integration of light microscopical and MRI data. Hum Brain Mapp 1998;6:339–47.

Streicher J, Weninger WJ, Muller GB. External marker-based automatic congruencing: a new method of 3D reconstruction from serial sections. Anat Rec 1997;248:583–602.

Uberti M, Liu Y, Dou H, Mosley RL, Gendelman HE, Boska M. Registration of in vivo MR to histology of rodent brains using blockface imaging. In: Medical imaging 2009: biomedical applications in molecular, structural, and functional imaging; 2009. p. 726213.

Vegh V, Yang Z, Tieng QM, Reutens DC. Multimodal image registration using stochastic differential equation optimization. In: International conference on image processing IEEE; 2010. p. 4385–8.

Wells I, William M, Viola P, Atsumi H, Nakajima S, Kikinis R. Multi-modal volume registration by maximization of mutual information. Med Image Anal 1996;1:35–51.

Wirtz S, Papenberg N, Fischer B, Schmitt O. Robust and staining-invariant elastic registration of a series of images from histologic slices. In: Medical imaging 2005: image processing; 2005. p. 1256–62.

Yang Z, Vegh V, Wang D, Reutens DC. Registration of histology and MR images using local rigid registration and differential evolution. In: Joint annual meeting ISMRM-ESMRMB ISMRM; 2010. p. 5100.

Yelnik J, Bardinet E, Dormont D, Malandain G, Ourselin S, Tand D, Karachi C, Ayache N, Cornu P, Agid Y. A three-dimensional, histological and deformable atlas of the human basal ganglia. I. Atlas construction based on immunohistochemical and MRI data. NeuroImage 2007;34:618–38.

Yushkevich P, Avants B, Ng L, Hawrylycz M, Burstein P, Zhang H, Gee J. 3D mouse brain reconstruction from histology using a coarse-to-fine approach. Utrecht, The Netherlands: Biomedical Image Registration; 2006, 230–7.

Zhu S, Ma KK. A new diamond search algorithm for fast block-matching motion estimation. IEEE Trans Image Process 2000;9:287.